Kinematic and dynamic simulation of an octopod robot controlled by different central pattern generators

Dariusz Grzelczyk [iD]**, Olga Szymanowska and Jan Awrejcewicz** [iD]

Abstract

The goal of the study was to perform both kinematic and dynamic simulation of an octopod robot walking on a flat and hard surface. To drive robot legs, different non-linear mechanical oscillators were employed as central pattern generators. Aside from using some well-known oscillators, a new model was proposed. Time series of robot's kinematic and dynamic locomotion parameters were computed and discussed. Displacement and velocity of the centre of gravity of the robot, ground reaction forces acting on the robot legs, as well as some aspects of energy consumption of a walking robot were analysed to assess the central pattern generators. The obtained kinematic and dynamic parameters showed some advantages of the applied generator. In particular, the gait of the robot was most stable when the robot was driven by the proposed central pattern generator model.

Introduction

Multi-legged robots are a type of mobile machines, which have gained significant importance in many engineering applications. They are inspired by the anatomy and locomotion of various animal species and have become the inspiration for numerous studies aimed at mobile robots. The growing interest in multi-legged robots is mainly caused by their ability to move on different, often uneven, terrains. The research on walking machines was started by McGhee and Frank,[1] who developed the first quadruped (four-legged) robot named 'Phoney Pony' in the 1960s. Since that time, numerous quadruped machines have been built.[2–7] Aside from them, hexapod (six-legged) robots, such as those presented in papers,[8–15] have been also developed and studied. An interesting state-of-the-art related to six-legged robots can be found in papers.[16,17]

Recently, octopod (eight-legged) robots have gained much research attention. To mention a few, a biomimetic SCORPION,[18] OctoRoACH,[19] or searching and rescuing Halluc II[20] octopods have been developed. The SCORPION robot has eight homogeneous legs and the main body consisting of three parts. The legs joints are controlled by typical DC motors with high gear transmission ratio. When it comes to OctoRoACH, its C-shape elastic legs are driven by independent drives located on each (two) sides of the robot, respectively. The motion of the device is realized by adjusting the speed of movement of the legs as well as the swing of the robot's mechanical tail. Halluc II is a robotic vehicle consisting of eight wheels and legs designed to drive or walk on a rugged terrain by using the wireless network and a system of cameras and sensors that monitor the distance to potential obstacles.

In comparison with wheeled vehicles, biologically inspired multi-legged robots are better at adapting to unknown and unstructured environments, which results, for instance, from their ability to overcome obstacles. Therefore, they can be used in places, where wheeled machines cannot fulfil their tasks. On the contrary, it should be mentioned that the leg–ground interaction of the walking robot varies over time, depending on the shape of the terrain. The amplitude of the

Department of Automation, Biomechanics and Mechatronics, Lodz University of Technology, Lodz, Poland

Corresponding author:
Dariusz Grzelczyk, Department of Automation, Biomechanics and Mechatronics, Lodz University of Technology, 1/15 Stefanowskiego Street, 90-924 Lodz, Poland.
Email: dariusz.grzelczyk@p.lodz.pl

ground reaction force during the leg–ground interaction has a great impact on the dynamic behaviour of joint torques and the energy consumption of the robot. The forces and torques in the joints of the robot legs should be reduced, which can protect individual components and the whole mechanical structure of the robot as well as improve their stability during walking. The choice of movements of the robot legs has also a significant influence on the kinematics and dynamics of the whole robot. A brief literature review of some existing control methods applied to various bionic legged robots is presented in paper.[21] For instance, the impedance control method has been widely employed to both the motor-driven[22,23] and the hydraulically driven legged robots.[24,25]

In general, multi-legged robots have poor energy efficiency. Therefore, performing typical tasks, such as locating and deactivating bombs, exploring planets, tasks in the underground mining, or security surveillance in prohibited areas, can be limited. In such situations, effective reduction of energy consumption would help the robot work for a longer time and minimize the size of actuators, thereby increasing the load-to-mass ratio and reducing the cost of the system. Hence, the reduction of power consumed by the walking robot, conducted by means of the appropriate control of robot legs, seems to be a good solution.

In this work, we focused on the modelling of the trajectory of the tip (end) of the robot leg and the analysis of the kinematic and dynamic parameters of the robot walking on a flat surface. The study was mainly motivated by the growing interest in legged robots[26–29] and the possible practical implementation of the octopod prototype in the future.

It should be noted that the present research can be extended with the use of achievements related to the control of robots walking on irregular terrains as systems of many degrees of freedom (DOFs), based on concepts reported in some recent papers. For instance, Deng et al.[30] proposed a novel control strategy for the multi-legged robot walking in dynamic environments. In their approach, the control strategy constantly changes the gait and the trajectory, adjusting them to different environments, tasks, and stability of the robot. As a result, a library of different kinds of gait was developed. According to the mentioned control method, a hierarchical architecture, consisting of man-machine interface, vision system, gait and trajectory planner, joint motion calculator, joint servo controller, compliance controller, and stability observer, were proposed.

In Wang et al.,[31] a central pattern generator (CPG) and a feed-forward neural network–based self-adaptive gait control method were presented for a crab-like robot moving on a complex terrain (more information on the CPG can be found in section "Control by CPGs" of this article). The proposed control system generates the waveform gait control of the robot. A tri-layer feed-forward neural network was constructed to establish the one-to-one mapping between rhythmic signals of the CPG and the joint angles. Based on the CPG system and the feed-forward neural network, two reflex mechanisms were put forward to realize the self-adaptive gait control on complex terrains.

Another approach worth mentioning is the sliding mode control (SMC).[32–34] It is one of the most popular non-linear strategies, which is characterized by a quick response and strong robustness. In the literature, one can find numerous sliding mode technique schemes that have been developed for different complex dynamical systems. In general, SMC changes the dynamics of a non-linear system by means of applying a discontinuous control signal which forces the system to slide along a cross-section of the system's normal behaviour.

The authors of this article have been studying the biologically inspired robots for some time. In Grzelczyk et al.,[17] a prototype of an insect-inspired six-legged robot for inspection and operational purposes was described. A detailed discussion on mechanical construction, electronic control system, and devices installed on the robot body was presented. Also, a CPG model based on the stick-slip oscillator was proposed. The obtained results, both numerical and experimental, exhibited some analogies in the characteristics of the investigated robot and animals (insects) met in nature.

In Grzelczyk et al.,[35] the kinematic, dynamic, and power consumption analysis was conducted for an updated version of the six-legged robot. The authors used the same stick-slip oscillator as in Grzelczyk et al.[17] A study of changes (fluctuations) in the centre of gravity (COG) of the robot, considered in the vertical and movement directions, was accompanied by the investigations of ground reaction forces acting on the robot legs as well as energy consumption of the walking hexapod. Time series of crucial kinematic and dynamic parameters of the locomotion of the robot were studied numerically and validated experimentally.

In contrast to the above-mentioned references, this article deals with kinematics and dynamics of a different multi-legged robot, that is, an octopod controlled by different CPGs. To conduct the study, the methods and models for control of the leg as well as models describing the kinematic and dynamic parameters of the robot were taken from Grzelczyk et al.[17,35] In addition, a new CPG model was developed and used. The model is based on a sine function and allows one to easily control the legs of the investigated mobile device. It can be generated by computer software or electronic circuits.[36] To conduct the numerical study, different CPGs as well as different parameters of the robot and a single stride were used. Eventually, the proposed CPG model yielded the most preferable kinematic and dynamic parameters in comparison with other models. It also turned out to produce the lowest energy consumption of the walking robot.

This article is organized as follows. In section 'Robot prototype', the studied octopod robot and its CAD model are introduced. The kinematic model of

the robot and its basic parameters are presented in section 'Kinematic model'. Section 'Control by CPGs' contains a brief literature review on CPG algorithms to control walking robots, followed by the definition of the proposed CPG model. Some interesting numerical simulations obtained for different configurations of a single robot leg, accompanied by kinematic and dynamic parameters of the whole walking robot, are illustrated and discussed in section 'Numerical results.' Conclusions from the study are outlined in section 'Conclusion'.

Robot prototype

In general, the design optimization of robots requires multiple modifications of their mechanical construction. Instead of developing prototypes, engineers can use virtual (computer-aided design (CAD)) models to perform numerical experiments, the results of which can be used at the next design step.

For the purpose of this study, a CAD model of the octopod (see Figure 1) was created in Inventor software. The size of the model is about 590 mm × 370 mm × 150 mm (length × width × height), while the total mass of the robot (estimated using Inventor) is 2.68 kg. The mechanical design comprises two main parts, that is, the main body and the legs. All eight legs are identical and their design was mainly inspired by the morphology of limbs of typical stick insects. They were reduced to three basic segments, that is, coxa, femur, and tibia, because other segments (i.e. trochanter and tarsus) are rarely used in a typical walking process.[37,38] The legs are symmetrically distributed on two sides of the robot body to avoid collisions between them. To create the model, a CAD three-joint leg mechanism, accompanied by definitions of links and joints described in Grzelczyk et al.,[17,35] was used. The designed robot is stable during standing and walking. In the future, a prototype of the device can be potentially adopted, for instance, for inspection and operating purposes.

In general, standard DC motors do not have high accuracy and they require calibration by the control system. Therefore, to drive the robot legs, 24 popular electric servomotors Tower Pro Mg995, which are controlled independently by the pulse-width-modulation (PWM) technique, were proposed. The actuators have a servo feedback (the inner closed loop feedback of the position control) and a proportional controller, which measures and controls joint angles based on the signal from the sensor (a potentiometer in each servo motor).

Kinematic model

Figure 2 presents a kinematic model of the investigated robot in two support configurations corresponding to different phases of the gait cycle. The octopod is placed in the global Cartesian coordinate system $Oxyz$, which
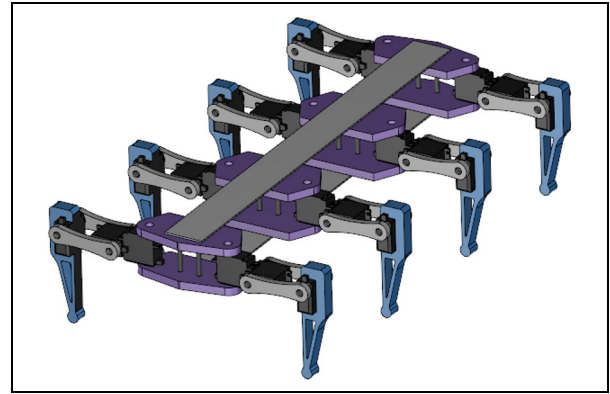

Figure 1. CAD model of the investigated octopod robot.[36]

is fixed to the ground, and Earth's gravity field ($g = 9.81$ m/s^2). In each gait phase, the robot stands on four legs, which form the support polygon (quadrangle). The robot body mass (excluding limbs) equals $M = 0.92$ kg. The legs are denoted by L1, L2, L3, L4 (on the left side of the robot) and R1, R2, R3, R4 (on the right side), respectively. It should be noted that the exact position of the COG of the robot slightly changes, depending on the configurations of the robot legs. To simplify the model, we assumed that the COG of the robot is located at the fixed point of the robot trunk (see Figure 2). Distances between the ground and the COG in different phases of the robot gait are denoted by $h_a(t)$, $h_b(t)$, respectively, whereas $R_{Li}(t)$ and $R_{Ri}(t)$ ($i = 1, 2, 3, 4$) state for ground reaction forces acting on the individual robot legs (see Figure 2). It was assumed that friction between robot legs and the ground is high enough to prevent the legs from sliding during locomotion.

The legs were arranged in two groups, that is, the group a consisting of R1, R3, L2, and L4 (Figure 2(a)) and the group b comprising L1, L3, R2, and R4 (Figure 2(b)). To control their motion, the same CPG model was used, but signals applied to each of the groups was in anti-phase. In other words, all legs of group a were in phase to one another and in anti-phase to the legs of group b (and vice versa). Each leg consisted of three links/segments corresponding to coxa, femur, and tibia of insects. A scheme of a single robot leg is presented in Figure 3. Links l_i ($i = 1, \ldots, 3$) and joints j_i form a kinematic scheme of the robot limb, which can be treated as a multibody system with 3 DOFs.[26] Moreover, the definitions of the angular positions $\varphi_i(t)$ of the segments l_i in the local Cartesian coordinate system $O'x'y'z'$ are also shown in Figure 3.

The respective masses m_i, lengths l_i, and distances a_i between the coordinates of joints j_i and mass centres of respective links were $m_1 = 0.116$ kg, $m_2 = 0.020$ kg, $m_3 = 0.084$ kg, $l_1 = 40$ mm, $l_2 = 70$ mm, $l_3 = 120$ mm, and $a_1 = 30$ mm, $a_2 = 35$ mm, $l_3 = 24$ mm. In the considered model, l_2 and l_3 correspond to femur and tibia, which are usually the longest segments of insects. More
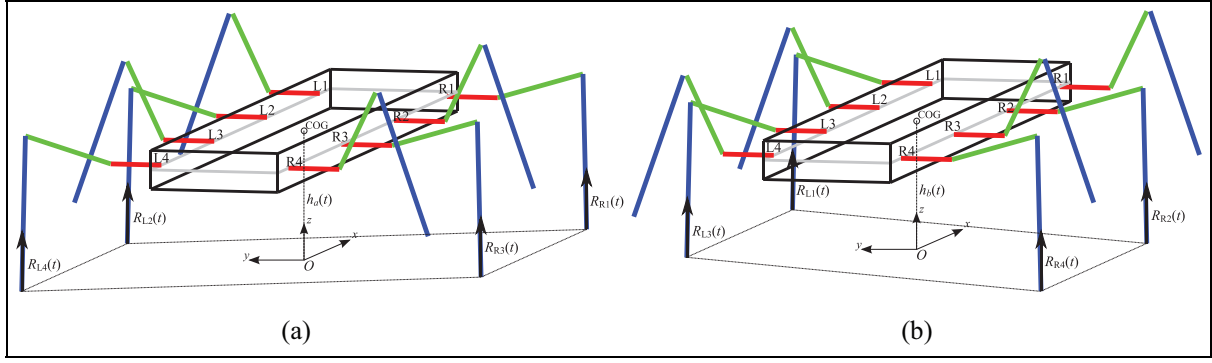
Figure 2. Kinematic model of the octopod robot in two support configurations: (a) support by the legs R1, R3, L2, and L4 and (b) support by the legs L1, L3, R2, and R4.

details on the relative proportions of lengths of the segments can be found, for instance, in Zhao et al.[39]

Forward kinematics, describing the relationship between the coordinates $x'(t)$, $y'(t)$, and $z'(t)$ of the supporting point (the tip of the robot leg) as functions of angles $\varphi_i(t)$ in the local coordinate system $O'x'y'z'$, has the form

$$\begin{cases} x'(t) = \cos\varphi_1(t)(l_1 + l_2\cos\varphi_2(t) + l_3\cos(\varphi_3(t) - \varphi_2(t))), \\ y'(t) = \sin\varphi_1(t)(l_1 + l_2\cos\varphi_2(t) + l_3\cos(\varphi_3(t) - \varphi_2(t))), \\ z'(t) = l_2\sin\varphi_2(t) - l_3\sin(\varphi_3(t) - \varphi_2(t)). \end{cases} \tag{1}$$

Inverse kinematics, which gives the dependence of articulated variables $\varphi_i(t)$ as functions of Cartesian variables $x'(t)$, $y'(t)$, and $z'(t)$, is given as follows

$$\varphi_1(t) = \begin{cases} \operatorname{atan}\left(\frac{y'(t)}{x'(t)}\right) & \text{if } x'(t) > 0 \\ \frac{\pi}{2} & \text{if } x'(t) = 0 \\ \pi - \operatorname{atan}\left(-\frac{y'(t)}{x'(t)}\right) & \text{if } x'(t) < 0 \end{cases} \tag{2}$$

$$\varphi_2(t) = \begin{cases} \alpha(t) + \beta(t) & \text{if } \sqrt{[x'(t)]^2 + [y'(t)]^2} - l_1 \geqslant 0 \\ \alpha(t) - \pi + \beta(t) & \text{if } \sqrt{[x'(t)]^2 + [y'(t)]^2} - l_1 < 0 \end{cases} \tag{3}$$

$$\varphi_3(t) = \operatorname{acos}\left(\frac{[c(t)]^2 - l_2^2 - l_3^2}{2l_2l_3}\right) \tag{4}$$

where $\alpha(t) = \operatorname{acos}((l_3^2 - l_2^2 - [c(t)]^2)/(-2l_2c(t)))$, $\beta(t) = \operatorname{atan}((z'(t))/(\sqrt{[x'(t)]^2 + [y'(t)]^2} - l_1))$, $[c(t)]^2 = [z'(t)]^2 + (\sqrt{[x'(t)]^2 + [y'(t)]^2} - l_1)^2$.

Control by CPGs

Walking of multi-legged robots is a complex task, which requires high coordination of all controlled legs, regardless of the type of the walking surface. For this purpose, the control system must select one of a variety of alternative movements. Furthermore, control of walking robots is usually based on two principles of biological control, namely, a CPG and a reflex. A reflex is a movement generated based on a sensor (a stimulus) in a feedback and reflex systems can be used in control systems of robots. For instance, in the Walknet robot,[40] the local sensory feedback in the legs and coupling between the control of neighbouring legs are sufficient to ensure a stable walk.

In this study, the other concept (CPG) was employed to develop the control method for the octopod legs. In general, CPGs are biological neural networks that produce rhythmic outputs in the absence of rhythmic input.[41] They are a source of tightly coupled patterns of neural activity that drive rhythmic motions in different biological processes like breathing, chewing, or walking. Studies have shown that CPGs have been detected in numerous vertebrate species,[42] including human.[43] The first CPG model was proposed in the 1980s by Cohen et al. who studied the dissection of a lamprey spinal cord.[44] Since that time, many researchers have been applying CPG algorithms (using linear/non-linear damped/non-damped mechanical oscillators with asymptotically stable limit cycles) to control different biologically inspired multi-legged walking robots. One can find numerous papers devoted to gait generation methods based on the CPGs.[26,45] Semini et al.[25] showed that a hexapod robot can perform different kinds of gaits by chaos control (however, the proposed model is difficult to be directly applied). An interesting literature review on CPGs can be found in the literature.[28–30]

Below, let us present three well-known and popular CPG models that can be applied to control leg movements of multi-legged robots. A Hopf oscillator, van der Pol oscillator, and Toda-Rayleigh lattice are non-linear mechanical oscillators, which are described by one-dimensional ordinary differential equations (ODEs). Two independent Hopf oscillators are governed by the following first-order ODEs

$$\begin{cases} \dot{X}_a(t) = (\mu - X_a^2(t) - Z_a^2(t))X_a(t) + \omega Z_a(t) \\ \dot{Z}_a(t) = (\mu - X_a^2(t) - Z_a^2(t))Z_a(t) - \omega X_a(t) \\ \dot{X}_b(t) = (\mu - X_b^2(t) - Z_b^2(t))X_b(t) + \omega Z_b(t) \\ \dot{Z}_b(t) = (\mu - X_b^2(t) - Z_b^2(t))Z_b(t) - \omega X_b(t) \end{cases} \tag{5}$$

Two independent van der Pol oscillators are described by the first-order ODEs

$$\begin{cases} \dot{X}_a(t) = Z_a(t) \\ \dot{Z}_a(t) = \mu\left(1 - X_a^2(t)\right)Z_a(t) - \omega^2 X_a(t) \\ \dot{X}_b(t) = Z_b(t) \\ \dot{Z}_b(t) = \mu\left(1 - X_b^2(t)\right)Z_b(t) - \omega^2 X_b(t) \end{cases} \quad (6)$$

while the Toda-Rayleigh lattice is governed by the first-order ODEs

$$\begin{cases} \dot{X}_a(t) = Z_a(t) \\ \dot{Z}_a(t) = \omega^2\left(e^{X_b(t)-X_a(t)} - e^{X_a(t)-X_b(t)}\right) + \mu\left(1 - Z_a^2(t)\right)Z_a(t) \\ \dot{X}_b(t) = Z_b(t) \\ \dot{Z}_b(t) = \omega^2\left(e^{X_a(t)-X_b(t)} - e^{X_b(t)-X_a(t)}\right) + \mu\left(1 - Z_b^2(t)\right)Z_b(t) \end{cases}$$
$$(7)$$

In the ODEs presented above, $X_a(t)$, $X_b(t)$, $Z_a(t)$, and $Z_b(t)$ are dimensionless variables, whereas ω and μ are constant dimensionless parameters. To control both leg groups (a and b), we used two independent CPG models (i.e. two Hopf oscillators and two van der Pol oscillators) in equations (5) and (6), starting from different initial conditions. However, all robot legs can also be controlled by the same CPG, as it has been already noted in section 'Kinematic model'.

Figure 4 presents stable orbits of the above-mentioned oscillators. The orbits were obtained for fixed values $\omega = 2$, $\mu = 6$ and different initial conditions (marked with squares). Numerical simulations were carried out by using the standard fourth-order Runge–Kutta method. It is clear that the results always converge to the same limit cycle (bold red curve), regardless of the initial values. Since the obtained trajectories of oscillations are stable irrespective of the initial conditions, these oscillators are often used to generate the trajectory of the tip of a robot leg. One can easily modify the shape and the period of a stable orbit by changing the values of μ and ω. As a consequence, one can control the parameters of a single robot stride. However, to control the robot leg, these trajectories must be converted to the workspace of the leg mechanism and then to the space of joints of the leg by means of using the inverse kinematics.

In the literature, one can easily find papers aimed at implementing the Hopf/van der Pol oscillators or the Toda-Rayleigh lattice to produce rhythmic biologically inspired movements. For instance, de Pina Filho and Dutra [46] have modelled a bipedal robot by means of a
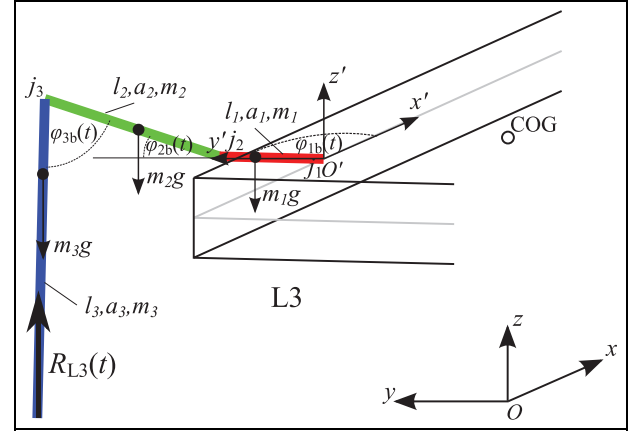

Figure 3. Schematic configuration of a single robot leg (L3 leg was used as an example).

coupled hybrid van der Pol–Rayleigh oscillators system. In Chen et al.[47] and Liu et al.,[48] in turn, Hopf oscillator–based models have been used to control quadruped and hexapod robots, respectively.

In this article, we propose a new generator model, motivated by the carried out study of a trajectory of a leg tip of real insects and various biologically inspired robots. The model is based on a sine function and is hereafter referred to as a SINE generator. It is governed by the following relations

$$X_a(t) = \begin{cases} -\dfrac{1}{\pi}\,\mathrm{modulo}(\omega t, \pi) & \text{if } 0 < \mathrm{modulo}(\omega t, 2\pi) \leq \dfrac{\pi}{2} \\ -\dfrac{1}{2} + \dfrac{1}{\pi}\,\mathrm{modulo}\left(\omega t - \dfrac{\pi}{2}, \pi\right) & \text{if } \dfrac{\pi}{2} < \mathrm{modulo}(\omega t, 2\pi) \leq \dfrac{3}{2}\pi \\ \dfrac{1}{2} - \dfrac{1}{\pi}\,\mathrm{modulo}\left(\omega t - \dfrac{3}{2}\pi, \pi\right) & \text{if } \dfrac{3}{2}\pi < \mathrm{modulo}(\omega t, 2\pi) \leq 2\pi \end{cases} \quad (8)$$

$$X_b(t) = -X_a(t) \quad (9)$$

$$Z_a(t) = \sin\left(\omega t - \dfrac{\pi}{2}\right) \cdot J\left(-\sin\left(\omega t + \dfrac{\pi}{2}\right)\right) \quad (10)$$

$$Z_b(t) = \sin\left(\omega t + \dfrac{\pi}{2}\right) \cdot J\left(-\sin\left(\omega t - \dfrac{\pi}{2}\right)\right) \quad (11)$$

where $J\left(-\sin\left(\omega t + (\pi/2)\right)\right)$ and $J\left(-\sin\left(\omega t - (\pi/2)\right)\right)$ are classical unit step functions defined as follows

$$J\left(-\sin\left(\omega t \pm \dfrac{\pi}{2}\right)\right) = \begin{cases} 1 \text{ if } -\sin\left(\omega t \pm \dfrac{\pi}{2}\right) > 0 \\ 0 \text{ if } -\sin\left(\omega t \pm \dfrac{\pi}{2}\right) \leq 0 \end{cases}$$
$$(12)$$

The stable orbits obtained for the proposed SINE generator are presented in Figure 5. The orbit presented in Figure 5(a) corresponds to the legs R1, R3, L2, and L4, while the orbit in Figure 5(b) corresponds to the legs L1, L3, R2, and R4. As can be seen from formulas (8) to (11), the periodic orbit in the space of variables $X_a(t) - Z_a(t)$ is in antiphase with respect to the orbit in the space of variables $X_b(t) - Z_b(t)$ (the phase shift equals π). Therefore, both periodic orbits in Figure 5 are the same. What is more, it can be easily noticed that the shape of the orbits in Figure 5 resembles the shape
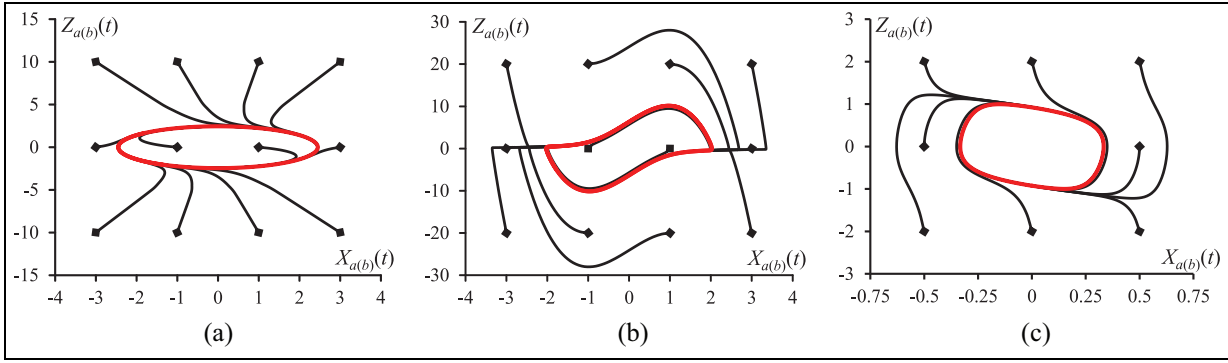
Figure 4. Phase trajectories of three typical non-linear oscillators for $\omega = 2$, $\mu = 6$ and various initial conditions: (a) Hopf oscillator, (b) van der Pol oscillator and (c) Toda–Rayleigh lattice.
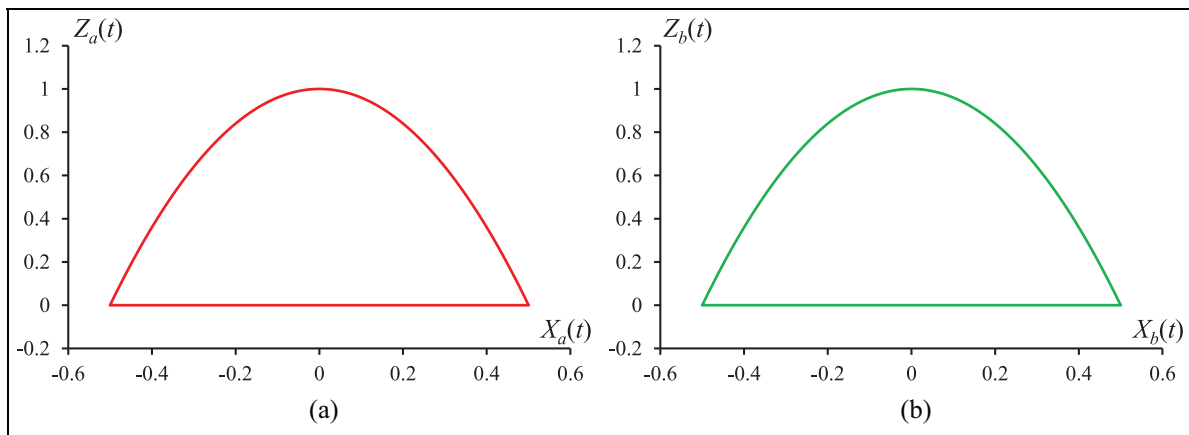

Figure 5. Phase trajectories of the proposed SINE generator: (a) $X_a(t) - Z_a(t)$ and (b) $X_b(t) - Z_b(t)$.

of the trajectory of the tip of a real stick insect leg presented in Dürr et al.[37] and Schilling et al.[38]

All the afore-presented phase trajectories can be used to control the tip of the robot leg. To modify the robot gait parameters, one can change phase trajectories by changing parameters of the used CPG model. Namely, the length and the height of a single stride can be controlled by means of the size and the shape of these trajectories and can be changed by multiplying the variables $X_a(t), Z_a(t)$ (which correspond to group a of the robot legs) and $X_b(t), Z_b(t)$ (which correspond to group b of the robot legs). The stride period, in turn, corresponds to the orbit period. Control parameters of a single robot stride can be obtained by converting the applied CPG signals to the workspace of the mechanism of the robot leg in the local coordinate system $O'x'y'z'$ in the following manner

$$\begin{cases} x'_{a(b)}(t) = l \cdot X_{a(b)}(t) \\ z'_{a(b)}(t) = h \cdot Z_{a(b)}(t) - L \end{cases} \tag{13}$$

where l, h are the length and the height of the single stride of the robot, respectively, whereas L states for the distance between the ground and the point of

attachment of the leg to the robot body (in the initial configuration the robot). One can easily modify the shape of the orbit by changing the values of l and h. Finally, the trajectories $x'_{a(b)}(t) - z'_{a(b)}(t)$ must be converted to the joints space of the legs by means of using the inverse kinematic relations (2)–(4).

Numeration of the octopod legs and a diagram showing schematically the considered robot gait are presented in Figure 6. Figure 7 illustrates the method used to generate signals (i.e. angular positions) for each leg of the robot. The periodic orbits $X_a(t) - Z_a(t)$ and $X_b(t) - Z_b(t)$, produced by the used CPG, are converted to the orbits $x'_a(t) - z'_a(t)$ and $x'_b(t) - z'_b(t)$ in the workspace of the robot leg $(y'_a(t), y'_b(t) = \text{const.})$, and then to the joints space $\varphi_{1a}(t)$, $\varphi_{2a}(t)$, $\varphi_{3a}(t)$ and $\varphi_{1b}(t)$, $\varphi_{2b}(t)$, $\varphi_{3b}(t)$, respectively. The angles $\varphi_{1a}(t)$, $\varphi_{2a}(t)$, $\varphi_{3a}(t)$ correspond to the robot legs R1, R3, L2, L4, whereas the angles $\varphi_{1b}(t)$, $\varphi_{2b}(t)$, $\varphi_{3b}(t)$ correspond to the legs L1, L3, R2, R4. The robot is supported by the legs of group a (see Figure 2(a)) in one phase and by the legs from group b (see Figure 2(b)) in the other one. As a result, the ground reaction forces act on different robot legs, depending on the gait phase.
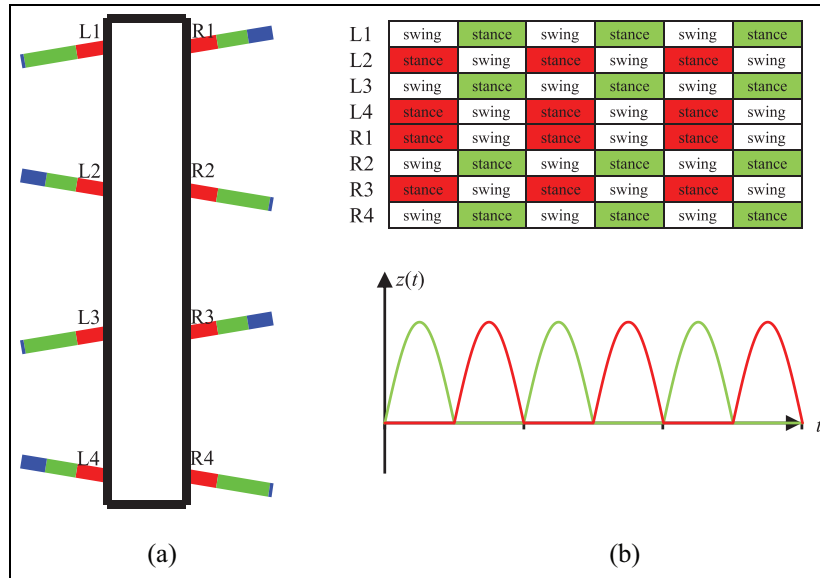
Figure 6. (a) Numeration of the octopod legs and (b) the diagram showing schematically the considered robot gait – white colour denotes the swing movement, while red and green colours denote the stance movements of the legs of the group *a* and *b*, respectively.
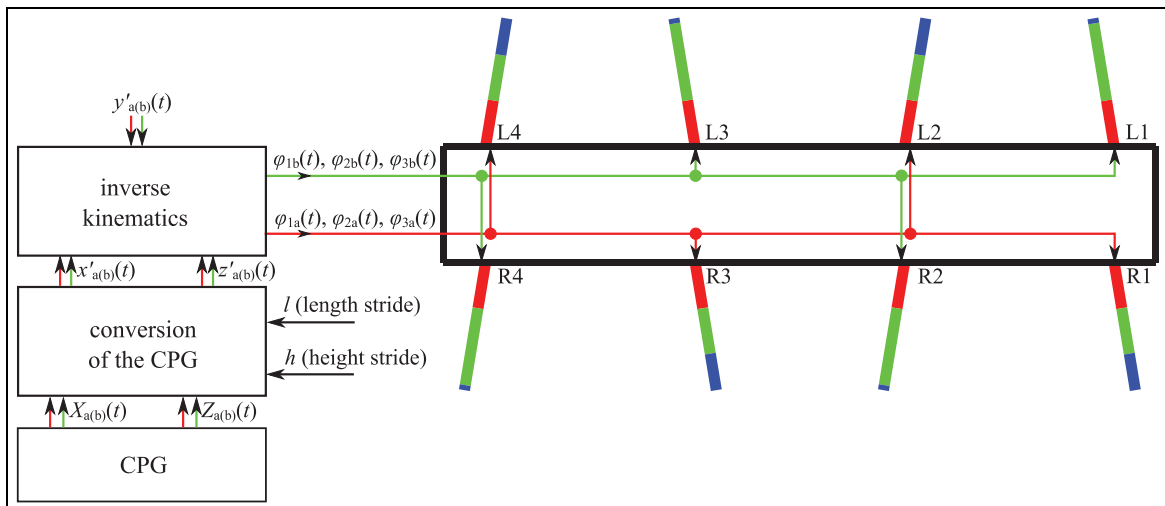

Figure 7. Method of generation of angular positions for individual joints of the octopod legs.

Figure 8 depicts the examples of stable orbits obtained for four considered CPG models. The orbits are presented in two manners, that is, in a normalized form (Figure 8(a)) and in the form scaled by the relations equation (13) to the workspace of the leg mechanism (Figure 8(b)). In numerical simulations, the variables $X_a(t)$, $X_b(t)$ were used to control the movement of the leg tip in the x-direction (direction of movement of the robot), whereas the variable $Z_a(t)$, $Z_b(t)$ to control the movement in the z-direction (vertical direction of the robot).

In general, insects oscillate when walking straight.[49] However, in multi-legged walking robots, the leg tips should move along straight lines parallel to both the course of the robot and the longitudinal axis of the robot body,[50] and the robot should translate without any oscillations. Therefore, in this study, the coordinates $y'_{a(b)}(t)$ were fixed in each phase of the gait (in this case, $y'_{a(b)}(t) = 110$ mm). Moreover, it should be emphasized that we neglected transient processes associated with initial and terminal phases of gait, and we focused only on a rhythmic gait. Transitions between different phases of gait are planned to be the investigated in future research.

Numerical results

In order to investigate the proposed CPG model and compare it with other models, numerical simulations were performed. For this purpose, the standard
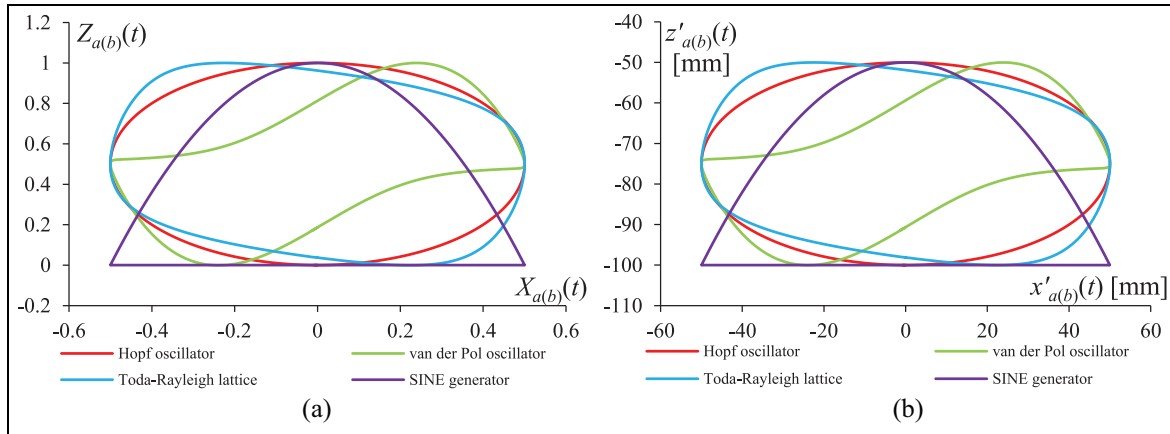
Figure 8. Stable orbits of the considered CPGs: (a) normalized periodic orbits and (b) the same orbits converted into the workspace of the leg mechanism (the stride length l = 100 mm, the stride height h = 50 mm, L = 100 mm).
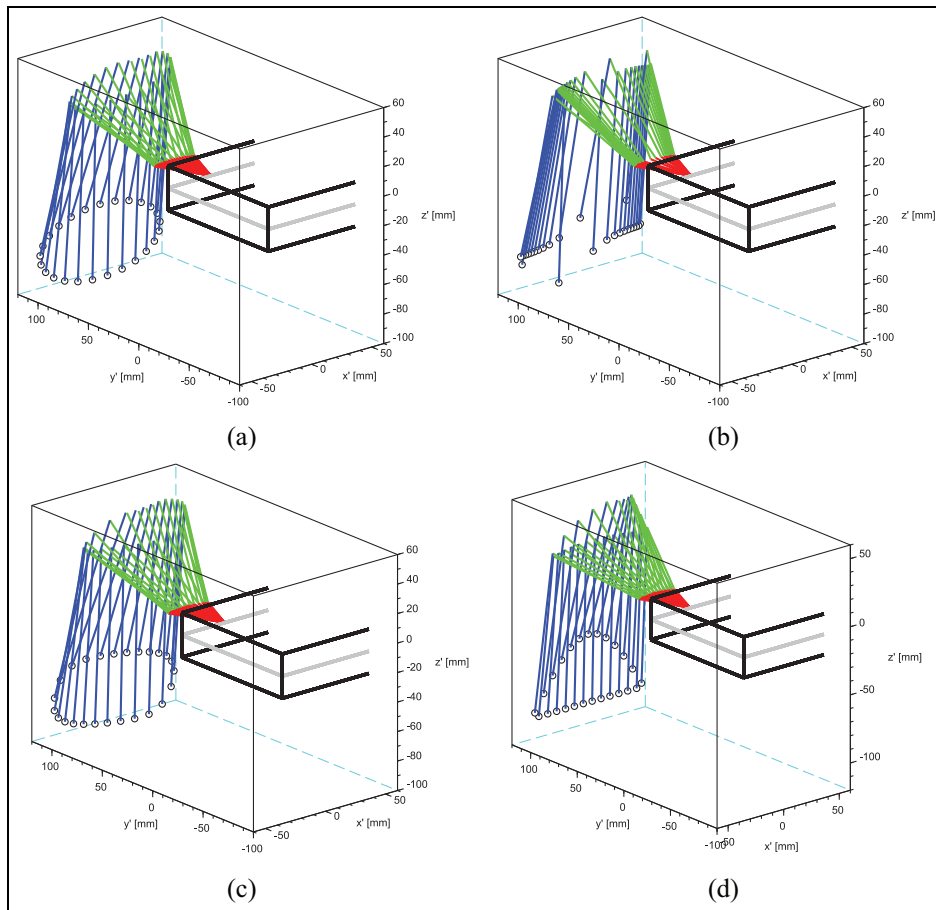

Figure 9. Visualization of the robot leg (L4) configurations and trajectory of the tips of legs, obtained for different CPGs: (a) Hopf oscillator, (b) van der Pol oscillator, (c) Toda-Rayleigh lattice and (d) SINE generator.

fourth-order Runge–Kutta method was implemented in Scilab. Also, the simulation model of the robot gait was developed with the use of the same software. The model was employed to obtain crucial parameters of motion of the walking robot. The initial parameters of robot gait were set as follows: the stride length l = 100 mm, the stride height h = 50 mm, L = 100 mm and the stride period T = 3 s (see Figure 8). Thus, the average speed of the robot in the forward direction was equal to 0.0667 m/s.
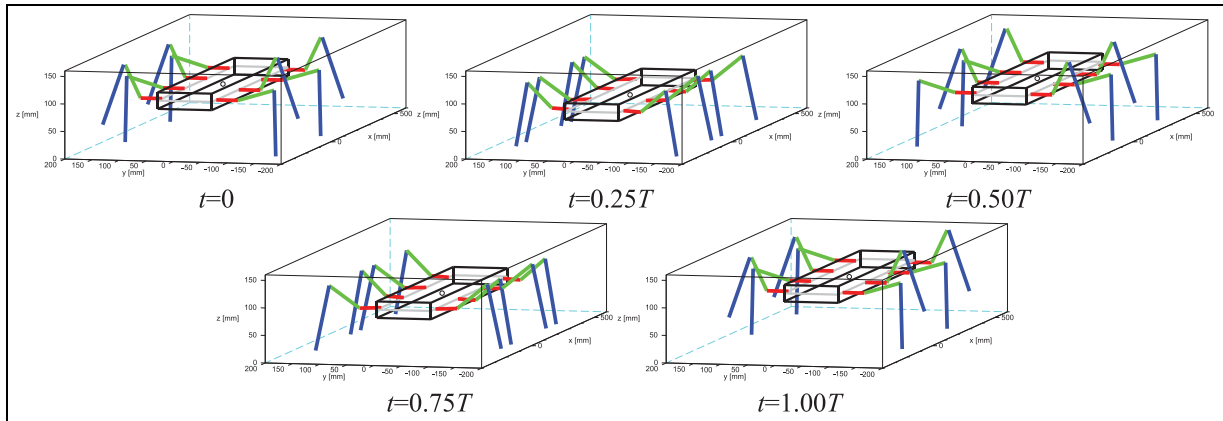
Figure 10. Configurations of robot legs in different gait phases (at regular time intervals), obtained for the octopod controlled by the Hopf oscillator.
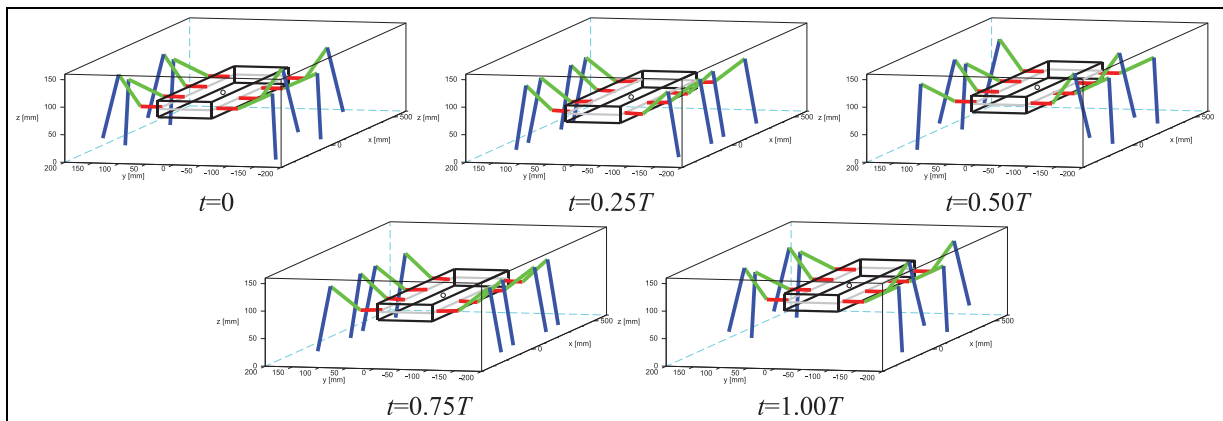

Figure 11. Configurations of robot legs in different gait phases (at regular time intervals), obtained for the octopod controlled by the van der Pol oscillator.
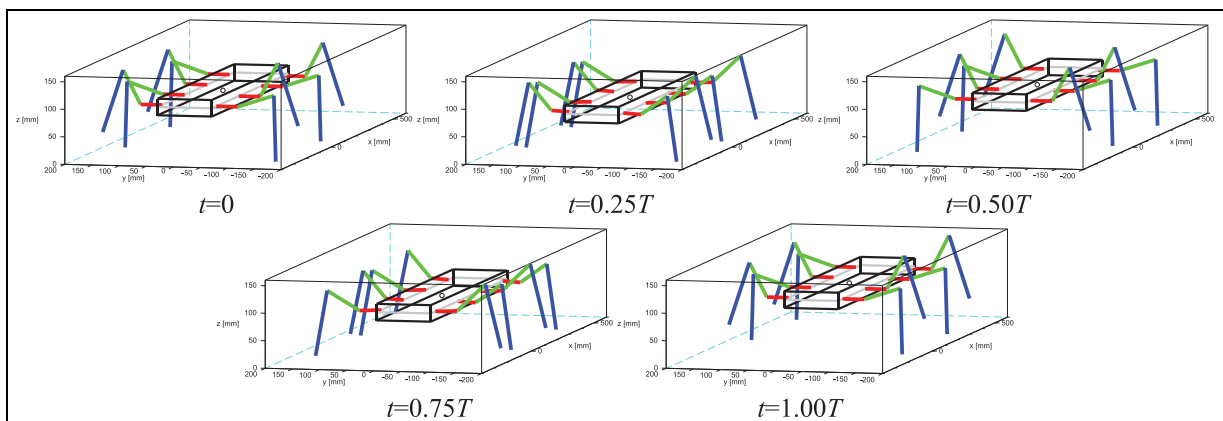

Figure 12. Configurations of robot legs in different gait phases (at regular time intervals), obtained for the octopod controlled by the Toda-Rayleigh lattice.

Figure 9 presents legs configurations and stable trajectories plotted by leg tips at regular time intervals, obtained for different CPGs. The figures explain how the investigated oscillators can be used to control a robot leg tip. In all presented cases, the leg tip plots the stable trajectory in the workspace of the leg mechanism. Moreover, the plotted trajectories are limited to a two-dimensional plane, which is parallel to the $x'z'$ plane of
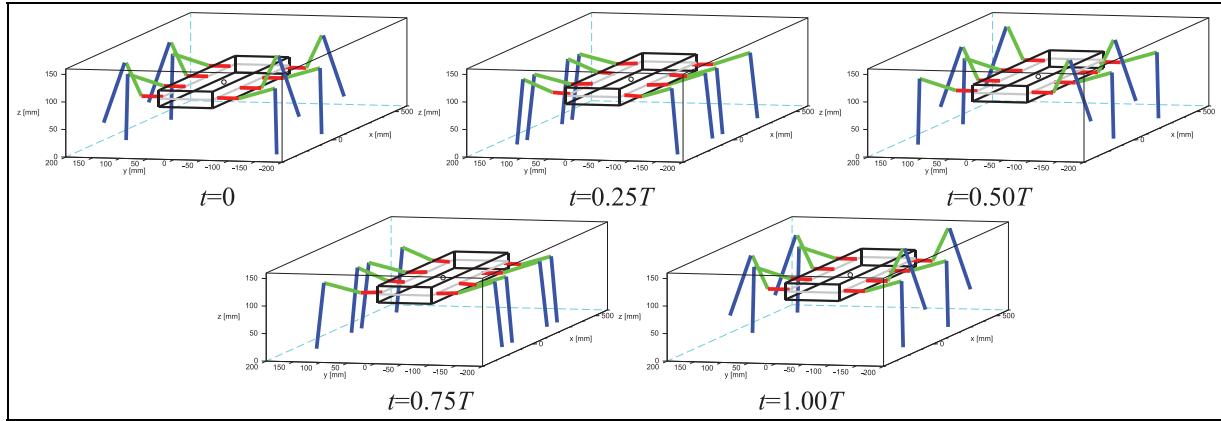
Figure 13. Configurations of robot legs in different gait phases (at regular time intervals), obtained for the octopod controlled by the SINE generator.

the local coordinate system. The presented numerical simulations refer to a single robot leg (in this case, the leg L4), and the results for other legs are similar.

As a result of applying the computed angular positions in the individual joints, the octopod robot moves in the forward direction. Below, some numerical simulations of the whole investigated octopod robot are reported and discussed. Figures 10–13 show configurations of the robot controlled by different CPGs, obtained at regular time intervals corresponding to consequent phases of a single stride of the robot. Moreover, side and top views of the configurations of robot legs, captured at regular time intervals in different phases of a robot stride, are also presented in Figure 14. An analysis of configurations of individual legs indicates that the distance between the COG of the robot and the ground changes significantly in some phases of the robot gait for the Hopf/van der Pol oscillators and the Toda-Rayleigh lattice. In the case of the proposed SINE generator, no fluctuations of the robot COG are observed in any phase of the robot motion.

To better illustrate the above observation, numerical trajectories of the robot's COG in the xz plane and time histories of kinematical parameters of the robot's COG were studied for all considered CPGs. Positions $z_C(t)$ and $x_C(t)$ of the robot's COG in the vertical and horizontal directions in the global coordinate system $Oxyz$ (see Figure 15) were calculated by the following relations

$$z_C(t) = \begin{cases} |z'_a(t)| & \text{if} \quad |z'_a(t)| \geqslant |z'_b(t)| \\ |z'_b(t)| & \text{if} \quad |z'_a(t)| < |z'_b(t)| \end{cases} \tag{14}$$

$$x_C(t) = \int \dot{x}_C(t) dt \tag{15}$$

where

$$\dot{x}_C(t) = \begin{cases} |\dot{x}'_a(t)| & \text{if} \quad |z'_a(t)| \geqslant |z'_b(t)| \\ |\dot{x}'_b(t)| & \text{if} \quad |z'_a(t)| < |z'_b(t)| \end{cases} \tag{16}$$

During normal gait, the curves of variation of the position of the gravity centre and acceleration of the

robot in the direction of movement should be possibly close to zero. Vertical fluctuations $z_C(t)$ of the robot's COG and trajectories plotted by tips of robot legs (group a– solid curves, b– dashed curves) are presented in Figure 16. One can clearly notice considerable fluctuations of the robot's COG in the case of the first three oscillators controlling the robot legs, on the contrary to the results for the SINE generator. The analysis of all CPG models studied in this article showed that the COG of the octopod robot moves up and down periodically (twice per one robot stride) in a range of a half of the stride height. This is not observed for the proposed SINE generator. Therefore, the proposed CPG model is advantageous, since it results in keeping the COG of the robot at a constant level in each gait phase.

In Figure 17, one can find curves of displacement of the robot's COG in both z and x directions, obtained for different CPGs. The corresponding curves of velocity (obtained by numerical differentiation of the displacement curves) are depicted in Figure 18. An analysis of the results presented in Figures 17 and 18 indicates that, aside from the fact that the distance between the COG of the robot and the ground significantly changes for typical oscillators, some periods of the robot motion are realized faster while other slower in the case of the van der Pol oscillator. Therefore, the above-mentioned fluctuations of the robot's COG are largest for this CPG model. In this case, one can observe the greatest unnecessary accelerations and decelerations of the COG of the robot in both forward and vertical directions. For the proposed SINE generator, fluctuations of the COG of the robot are not observed in any phase of robot movement. It should be also noted that the velocities of the robot's COG were obtained by simple numerical differentiation of the displacement variations, and therefore can slightly differ from reality. However, one can notice a tendency of results, which is similar to the one observed in the case of displacement curves. Namely, the obtained results indicate characteristic fluctuations of the velocity of the
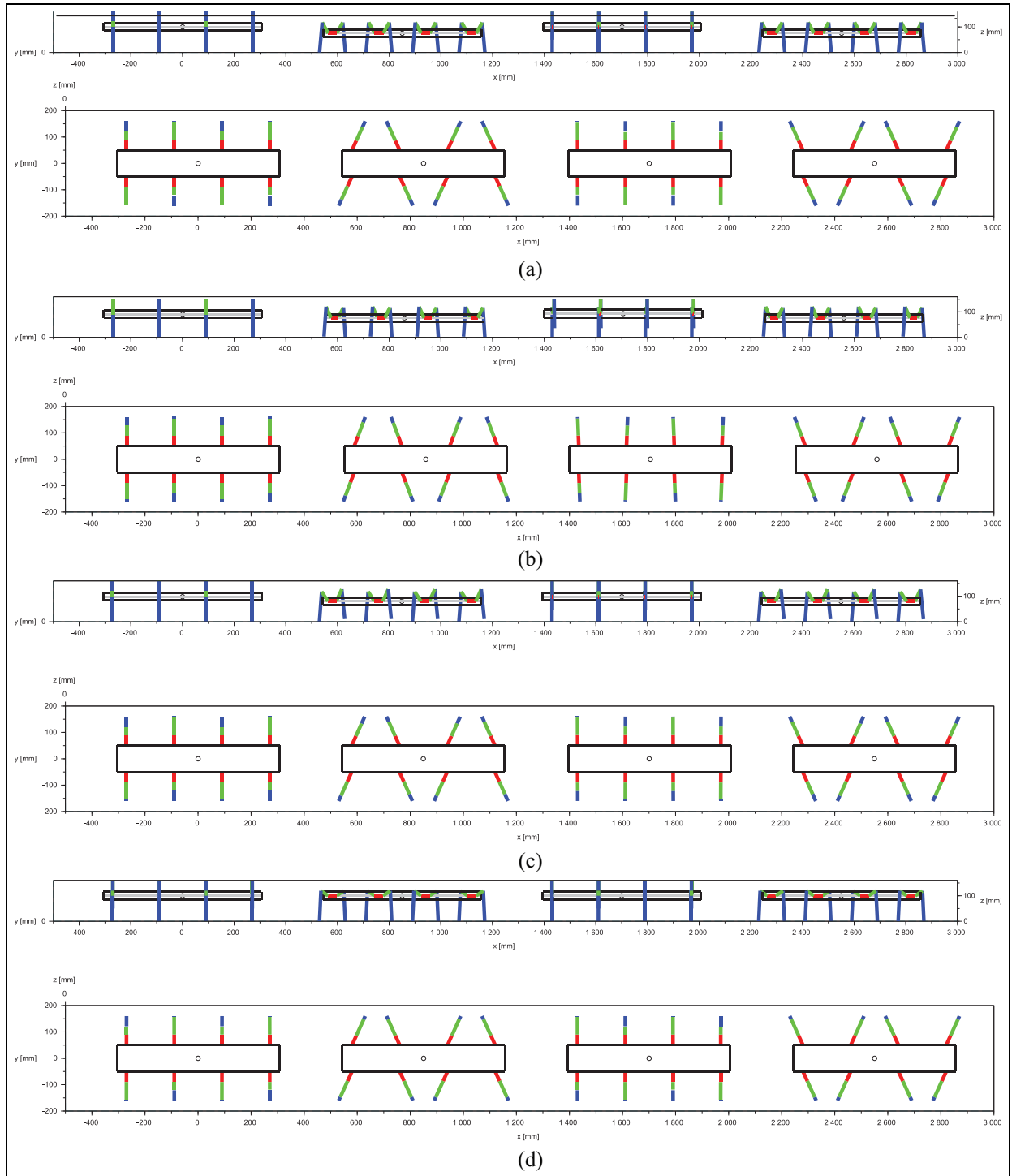
Figure 14. Side and top views of configurations of robot legs, obtained for different gait phases at regular time intervals ($t = 0$, $t = 4.25$ *T*, $t = 8.50$ *T* and $t = 12.75$ *T*– from the left to the right) for the octopod controlled by different CPGs: (a) Hopf oscillator, (b) van der Pol oscillator, (c) Toda-Rayleigh lattice and (d) SINE generator.

robot (two per one robot stride) for the first three typical oscillators/CPG models but not for the proposed CPG model.

It should be mentioned that variations in the displacement and velocity of the robot's COG, presented in Figures 15–18, have a great influence on the contact forces acting on robot legs due to vertical acceleration/deceleration of the COG. By virtue of these variations, the values of reaction forces oscillate (increase and decrease) around the reaction force resulting from the weight of the robot. As a consequence, most frequent and largest oscillations of contact forces are expected
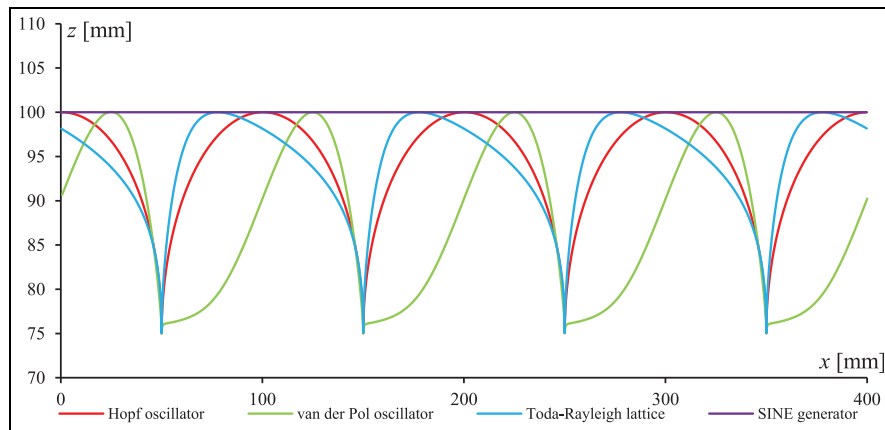
Figure 15. Trajectories plotted by the COG of the robot in the *xz* plane of the global coordinate system, obtained numerically for different CPGs.
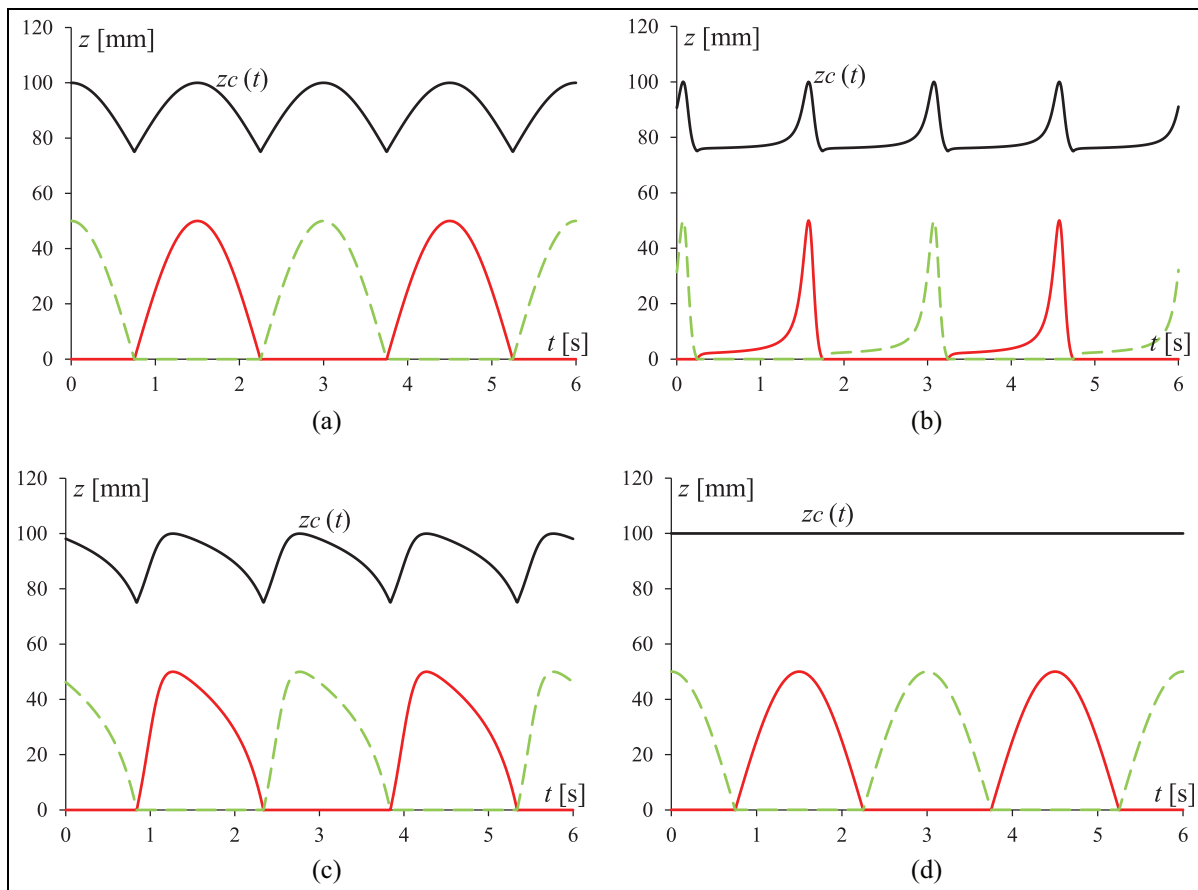

Figure 16. Fluctuations $z_C(t)$ of the robot's centre of gravity and trajectories plotted by robot legs for different CPGs (solid curves – group *a*, dashed curves – group *b*): (a) Hopf oscillator, (b) van der Pol oscillator, (c) Toda-Rayleigh lattice and (d) SINE generator.

for the van der Pol oscillator, while the smallest variations in contact forces should be obtained for the proposed SINE generator.

Power consumption is one of the most important factors and operational restrictions that must be taken into account in the development of autonomous walking machines. In some cases, the development of walking robots has been limited by too high energy consumption of prototypes. For the last three to four decades, many researchers have been creating and investigating methods for optimisation of power consumption of walking robots.[51–56] Variations in the robot's COG as well as in the speed/velocity and acceleration in the direction of the robot movement significantly influence the energy demand of a walking robot, that is, the higher the variations, the higher is the energy demand. Therefore, the above-mentioned variations should be as small as possible, and hence the
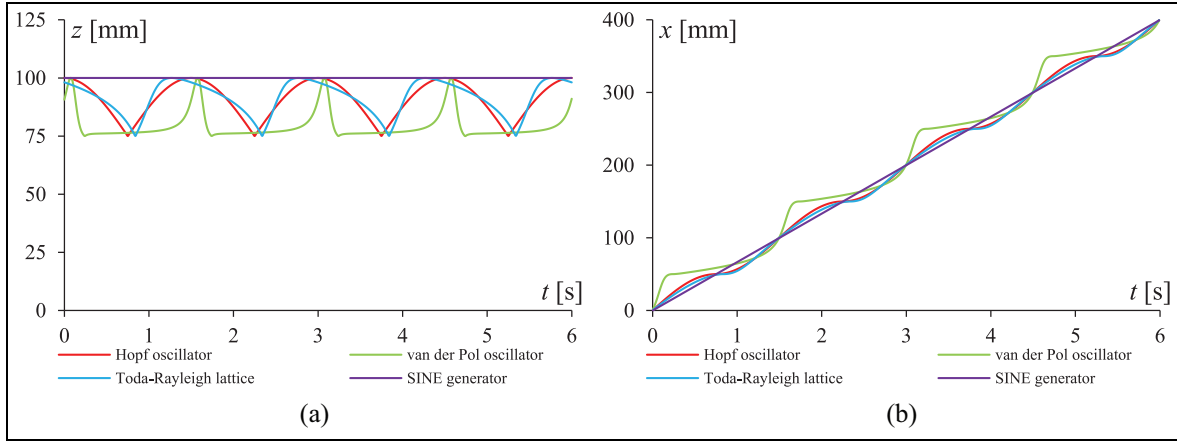
Figure 17. Fluctuations of curves of displacement of the robot's centre of gravity, obtained numerically for different CPGs: (a) in the z direction and (b) in the x direction.
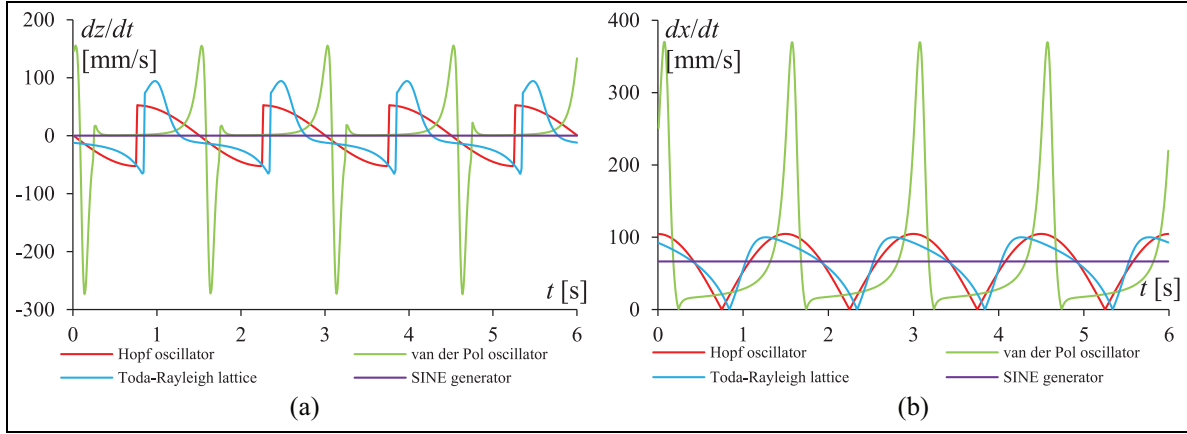

Figure 18. Fluctuations of curves of velocity of the robot's centre of gravity, obtained numerically for different CPGs: (a) in the z direction and (b) in the x direction.

proposed SINE CPG model is most optimal from the point of view of energy consumption.

As it has been mentioned before, fluctuations of the position of the COG of the octopod, caused by changes in velocity of vertical movement of the robot, have a significant impact on contact forces acting on each robot leg. In our study, these forces were estimated based on the concept of inverse dynamics implemented in Mathematica. Equations for translatory motion in the vertical direction z of the global coordinate system $Oxyz$ (optionally, with additional load of mass M_L transported by the robot) can be written in the following form

$$(M + M_L)\ddot{z}_C(t) + \sum_{j=1}^{4}\sum_{i=1}^{3} m_i\ddot{z}_{iRj}(t) + \sum_{j=1}^{4}\sum_{i=1}^{3} m_i\ddot{z}_{iLj}(t)$$
$$+ \left(M + M_L + 8\sum_{i=1}^{3} m_i\right)g = R_{R1}(t)$$
$$+ R_{R3}(t) + R_{L2}(t) + R_{L4}(t)$$

$$(17)$$

for $h_a(t) \geqslant h_b(t)$, and

$$(M + M_L)\ddot{z}_C(t) + \sum_{j=1}^{4}\sum_{i=1}^{3} m_i\ddot{z}_{iRj}(t) + \sum_{j=1}^{4}\sum_{i=1}^{3} m_i\ddot{z}_{iLj}(t)$$
$$+ \left(M + M_L + 8\sum_{i=1}^{3} m_i\right)g = R_{L1}(t) + R_{L3}(t)$$
$$+ R_{R2}(t) + R_{R4}(t)$$

$$(18)$$

for $h_a(t) < h_b(t)$. In equations (17)–(18), $\ddot{z}_{iRj}(t)$ and $\ddot{z}_{iLj}(t)$ denote positions of centres of masses of the ith links of the Rjth and Ljth legs, respectively, whereas

$$h_a(t) = |l_2 \sin \varphi_{2a}(t) - l_3 \sin (\varphi_{3a}(t) - \varphi_{2a}(t))| \quad (19)$$
$$h_b(t) = |l_2 \sin \varphi_{2b}(t) - l_3 \sin (\varphi_{3b}(t) - \varphi_{2b}(t))| \quad (20)$$

Both equations (17) and (18) have four variables (i.e. ground reaction forces acting on the individual robot legs). Due to a symmetrical distribution of the robot legs, the lack of the rotation of the robot body during gait, and partial compensation of legs mutual
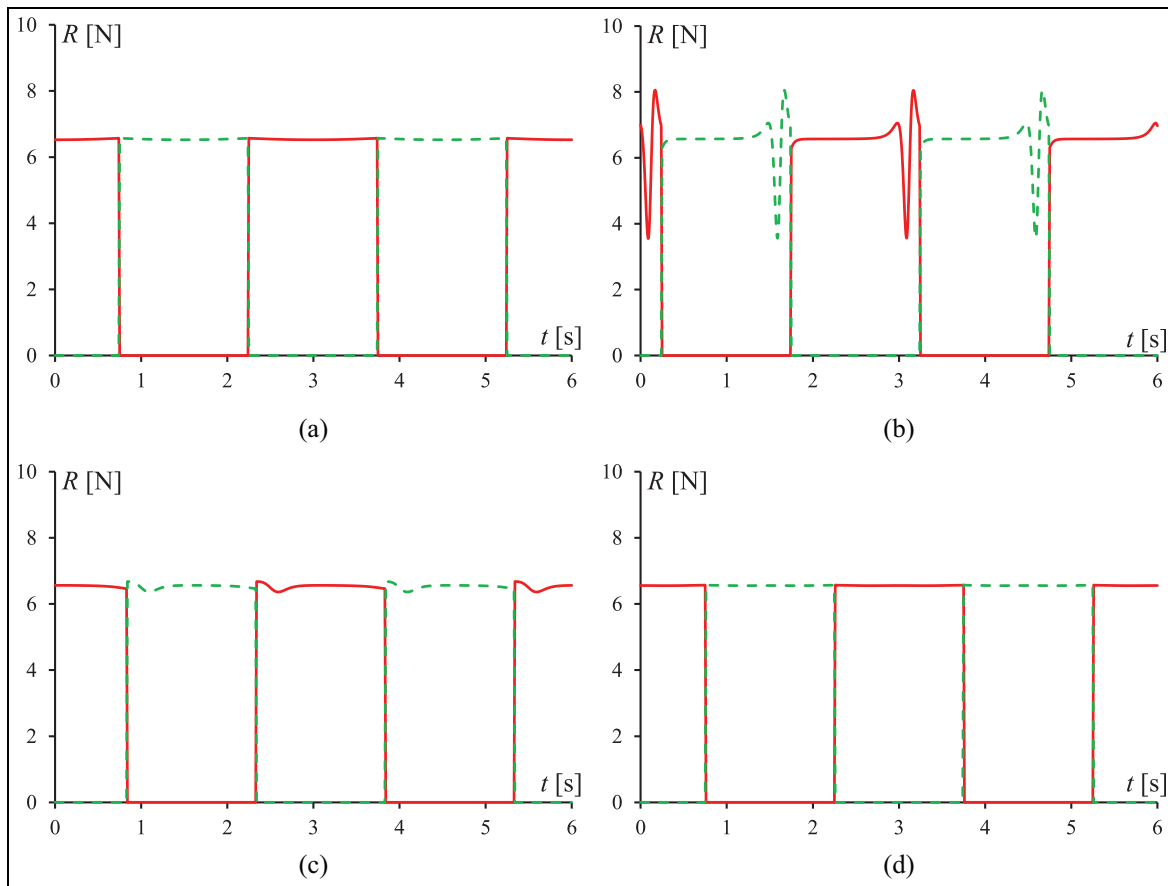
Figure 19. Time histories of the ground reaction forces (red solid curves denote $R_a(t)$, whereas green dashed curves denote $R_b(t)$): (a) Hopf oscillator, (b) van der Pol oscillator, (c) Toda-Rayleigh lattice, and (d) SINE generator.

movements, we assumed that $R_{R1}(t) = R_{R3}(t) = R_{L2}(t) = R_{L4}(t) = R_a(t)$ and $R_{L1}(t) = R_{L3}(t) = R_{R2}(t) = R_{R4}(t) = R_b(t)$ for simplification reasons. Owing to this assumption, it was possible to determine the average values of forces acting on the legs of the walking robot. It should be mentioned that although the adopted assumptions simplify the dynamic model of the robot, the obtained results are sufficient to compare the key dynamic parameters of the investigated robot during gait controlled by different CPG models.

Figure 19 shows time histories of ground reaction forces acting on robot legs for different CPG models. Owing to the assumptions described above, the values of the reaction force $R(t)$ acting between the ground and each robot leg are the same for all legs. The values of $R(t)$ oscillate (increase and decrease) around reaction force resulting from the weight of the robot (which equals about 6.6 N). The most frequent and largest oscillations of contact forces occur in the case of the van der Pol oscillator, while the smallest fluctuations are observed for the proposed SINE generator. Similar qualitative conclusions can be also achieved for other stride periods.

The results presented in Figure 19 were obtained by the appropriate double differentiation of variations in the displacement of the robot's COG and displacements of the links of the robot legs (their masses were taken into account). However, the exact values of contact forces at the moment of changing of supporting legs also strongly depend on the parameters of the contacting surfaces (i.e. tips of the robot legs and the ground) as well as the construction of the whole robot. The applied contact model also has an impact on the obtained ground reaction forces. However, the mentioned contact problem was not considered in detail in this study.

Moreover, we also investigated the influence of the parameters of the robot gait (i.e. the period T, the length l, and the height h of a single stride, as well as additional load M_L transported by the robot) on the relative oscillations of forces acting on robot legs during walking. Figure 20 presents values of the coefficient η, which describes the relative fluctuations of the ground reaction force (during interaction of the robot leg with the ground) with respect to the force resulting from gravity, defined as follows
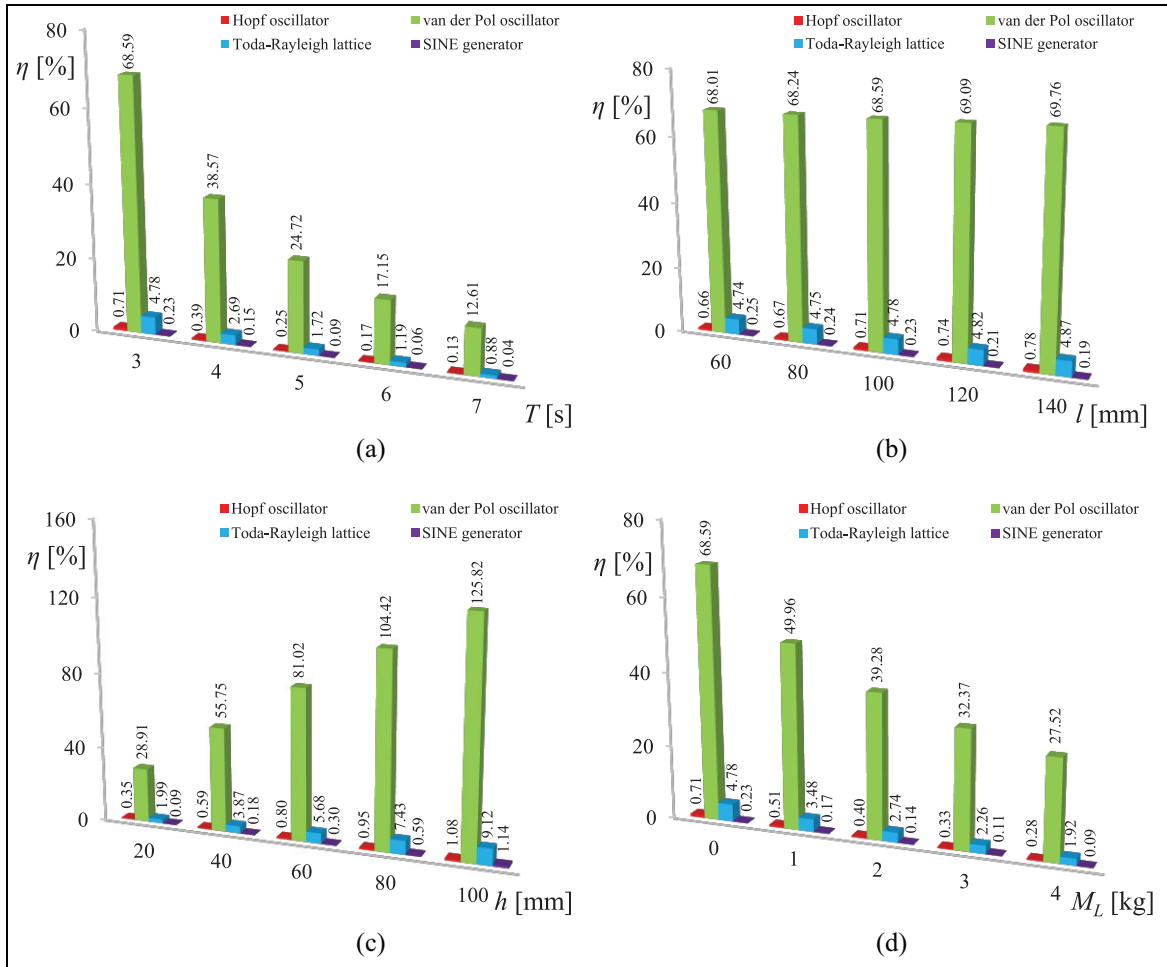
Figure 20. Values of the parameter η, which characterizes the relative fluctuation of ground reaction forces acting on the robot leg for different CPGs.

$$\eta = \frac{R_{\max} - R_{\min}}{R_{\text{gravity}}} \cdot 100\% \qquad (21)$$

calculated for different CPG models. Due to assumptions adopted, the coefficient η has the same value for all robot legs.

The analysis of the results presented in Figure 20 shows that for all presented cases, the highest values of the coefficient η are obtained for the van der Pol oscillator. As it has been already mentioned, this is mainly due to large fluctuations of the robot vertical velocity. Both the Hopf oscillator and the Toda-Rayleigh lattice working as a CPG also cause vertical fluctuations of the robot's COG, but the changes are much smaller than in the case of the van der Pol oscillator. Therefore, values of the coefficient η are smaller in these cases. The least significant differences in forces acting on robot legs (the smallest values of η) are observed in the case of the proposed CPG model (SINE generator). For this model, the vertical position of robot's COG does not change, and one can notice only slight

oscillations of COGs of segments of masses m_2 and m_3, while the main robot body of the mass M (optionally with additional mass M_L) as well as segments of the mass m_1 do not change their vertical position during gait.

Figure 20(a) shows that the value of η decreases with the increase in the period T of a single stride of the robot, which results from lower velocities of the robot's COG in the vertical direction. The influence of the stride length l on the parameter η can be treated as insignificant due to similar amplitudes and frequencies of changes in the vertical position of individual legs (see Figure 20(b)), but the impact of the stride height h is much higher. Namely, a higher value of h causes higher fluctuations of vertical positions and velocities of individual robot elements. As a result, higher values of η are obtained, which is shown in Figure 20(c). In turn, the results depicted in Figure 20(d) illustrate that the value of η decreases with the increase in the additional mass carried by the robot. However, this appears to be caused by the increase in

the value of $R_{gravity}$, which also increases with the increase in M_L.

Conclusion

A biologically inspired model of the octopod robot was presented and modelled to study kinematic and dynamic parameters of the robot locomotion and some aspects of robot power consumption analysis. The gait of the studied machine on a flat and hard ground was generated by four different CPG models, including three typical oscillators accompanied by the new, proposed one. The ground was assumed to be relatively hard to generate greater contact forces between the robot leg and the ground.

The proposed SINE generator, which is based on the sine function, is relatively simple in comparison with other control methods found in the literature (for instance, solving of a non-linear differential equations is not required). Furthermore, a detailed analysis of results shows that for the Hopf oscillator, van der Pol oscillator, and the Toda-Rayleigh lattice, the change in the parameter ω affects both the frequency and the amplitude of the oscillations. In the case of the proposed CPG model, the change in the value of this parameter has an influence only on the change in the frequency of oscillations, which makes it easier to control the parameters of the walking robot.

For comparison purposes, it is especially useful to study the case when the robot walks on flat, regular surfaces. The performed analysis shows that the applied CPG model significantly influences both kinematic and dynamical parameters of the robot gait. The CPG model based on the van der Pol oscillator appears to be the worst to control the gait of the octopod robot because it produces the largest unnecessary (and unwanted) changes in the velocity of the robot, both in the vertical and horizontal (movement) directions of the robot. These changes have a great impact on the energy consumption of the walking robot, and thus both the variations in the COG and acceleration of the robot in the direction of robot movement should be as close to zero as possible during normal gait. The proposed CPG model does not produce the unnecessary fluctuations of the COG of the robot nor variations in the acceleration/deceleration in the direction of the robot movement. Therefore, the proposed generator appears to be more efficient with respect to the energy demand in comparison with other investigated CPGs.

In conclusion, the configurations of the robot leg and trajectories plotted by the leg tip in the case of the proposed CPG model indicate good analogies between the movements of the simulated walking robot leg and the movements of the animal leg. Moreover, advantages of the employed CPG model have been clearly emphasized in this article, especially with regard to the kinematic parameters (i.e. displacement and velocity of the whole robot) and dynamic parameters (i.e. ground reaction forces and overloads acting on the robot legs). This article contains important information regarding kinematic and dynamic parameters that can be used to control not only the robot legs but also the whole robot. This is why the results of the study can be useful for further analysis of the strength and structural stability of the whole robot and robot legs as well as a trouble-free operation or extending the lifetime of robots.

It is also important to mention the limitations of the study conducted. Namely, to investigate the dynamics of the multi-legged robot properly, a more realistic model of contact between all segments of the robot is required, including both normal and tangential components of the forces as well as impact and friction at all contact interfaces. This issue was not the subject of this work. However, the obtained forces make it possible to clearly conclude that the proposed CPG model has significant advantages in comparison to other models presented in this work. What is more, although fluctuations of the robot's COG are negligible in the case of the proposed algorithm, there may occur some deviations of the robot's COG from the assumed trajectory in a real robot control system, which can be caused, for example, by control errors and dynamics of drives installed in individual robot joints. The authors believe that further research in this area may be interesting and should constitute the next stage of the work. Other, more detailed cases of the robot gait and control of the position of the robot moving on an irregular terrain is also worth taking into account in the future research activities. Other directions of development include the use of the SMC technique to study the control problem of the investigated octopod and examination of transitions between different phases of gait.

ORCID iD

Dariusz Grzelczyk https://orcid.org/0000-0002-7638-6582
Jan Awrejcewicz https://orcid.org/0000-0003-0387-921X

References

1. McGhee RB and Frank AA. On the stability properties of quadruped creeping gaits. *Math Biosci* 1968; 3: 331–351.

2. Galvez JA, Estremera J and De Santos PG. A new legged-robot configuration for research in force distribution. *Mechatronics* 2003; 13: 907–932.

3. Fukuoka Y, Kimura H, Hada Y, et al. Adaptive dynamic walking of a quadruped robot 'Tekken' on irregular terrain using a neural system model. In: *Proceedings of the IEEE international conference on robotics and automation (Cat. No.03CH37422)*, Taipei, Taiwan, 14–19 September 2003, vol. 2, pp.2037–2042. New York: IEEE.

4. Spenneberg D, Strack A, Hilljegerdes J, et al. Aramies: a four-legged climbing and walking robot. Eur Space Agency, 2005, https://pdfs.semanticscholar.org/ea12/c58109e645af9500e34e792bc3f36d145c3c.pdf

5. Raibert M, Blankespoor K, Nelson G, et al. BigDog, the Rough-Terrain Quadruped Robot. *IFAC Proc Vol* 2008; 41: 10822–10825.

6. Rutishauser S, Sprowitz A, Righetti L, et al. Passive compliant quadruped robot using central pattern generators for locomotion control. In: *Proceedings of the 2nd IEEE RAS & EMBS International Conference on Biomedical Robotics and Biomechatronics*, Scottsdale, AZ, 19–22 October 2008, pp.710–715.

7. Kato K and Hirose S. Development of the quadruped walking robot, TITAN-IX -mechanical design concept and application for the humanitarian de-mining robot. *Adv Robot* 2001; 15: 191–204.

8. Cobano JA, Estremera J and Gonzalez De, Santos P. Accurate tracking of legged robots on natural terrain. *Auton Robot* 2010; 28: 231–244.

9. Soyguder S and Alli H. Kinematic and dynamic analysis of a hexapod walking–running–bounding gaits robot and control actions. *Comput Electr Eng* 2012; 38: 444–458.

10. Ozkul MC, Saranli A and Yazicioglu Y. Acoustic surface perception from naturally occurring step sounds of a dexterous hexapod robot. *Mech Syst Signal Pr* 2013; 40: 178–193.

11. Zhang H, Liu Y, Zhao J, et al. Development of a bionic hexapod robot for walking on unstructured terrain. *J Bionic Eng* 2014; 11: 176–187.

12. Agheli M, Qu L and Nestinger SS. SHeRo: scalable hexapod robot for maintenance, repair, and operations. *Robot Cim: Int Manuf* 2014; 30: 478–488.

13. Henrey M, Ahmed A, Boscariol P, et al. Abigaille-III: a versatile, bioinspired hexapod for scaling smooth vertical surfaces. *J Bionic Eng* 2014; 11: 1–17.

14. Nelson GM, Quinn RD, Bachmann RJ, et al. Design and simulation of a cockroach-like hexapod robot. In: *Proceedings of the international conference on robotics and automation*, Albuquerque, NM, 25 April 1997, pp.3–8. New York: IEEE.

15. Saranli U, Buehler M and Koditschek DE. RHex: a simple and highly mobile hexapod robot. *Int J Robot Res* 2001; 20: 616–631.

16. Chen X, Wang LQ, Ye XF, et al. Prototype development and gait planning of biologically inspired multi-legged crablike robot. *Mechatronics* 2013; 23: 429–444.

17. Grzelczyk D, Stańczyk B and Awrejcewicz J. Prototype, control system architecture and controlling of the hexapod legs with nonlinear stick-slip vibrations. *Mechatronics* 2016; 37: 63–78.

18. Klaassen B, Linnemann R, Spenneberg D, et al. Biomimetic walking robot SCORPION: control and modeling. *Robot Auton Syst* 2002; 41: 69–76.

19. Pullin AO, Kohut NJ, Zarrouk D, et al. Dynamic turning of 13 cm robot comparing tail and differential drive. In: *Proceedings of the IEEE international conference on robotics and automation*, Saint Paul, MN, 14–18 May 2012, pp.5086–5093. New York: IEEE.

20. Future robotics technology center Chiba institute of technology HallucII: The Next-Generation Robotic Vehicle, 2007, https://www.furo.org/en/works/halluc2/halluc2.html (accessed 16 February 2018)

21. Ba K, Yu B, Gao Z, et al. Parameters sensitivity analysis of position-based impedance control for bionic legged robots' HDU. *Appl Sci* 2017; 7: 1035.

22. Poulakakis I, Smith JA and Buehler M. Modeling and experiments of untethered quadrupedal running with a bounding gait: the scout II robot. *Int J Robot Res* 2005; 24: 239–256.

23. Kimura H, Fukuoka Y and Cohen AH. Adaptive dynamic walking of a quadruped robot on natural ground based on biological concepts. *Int J Robot Res* 2007; 26: 475–490.

24. Rong X, Li Y, Ruan J, et al. Design and simulation for a hydraulic actuated quadruped robot. *J Mech Sci Technol* 2012; 26: 1171–1177.

25. Semini C, Barasuol V, Boaventura T, et al. Towards versatile legged robots through active impedance control. *Int J Robot Res* 2015; 34: 1003–1020.

26. Steingrube S, Timme M, Wörgötter F, et al. Self-organized adaptation of a simple neural circuit enables complex robot behaviour. *Nat Phys* 2010; 6: 224–230.

27. Grzelczyk D, Stańczyk B and Awrejcewicz J. Estimation of the contact forces between the hexapod legs and the ground during walking in the tripod gait. *Vib Phys Syst* 2016; 27: 107–114.

28. Roy SS and Pratihar DK. Kinematics, dynamics and power consumption analyses for turning motion of a six-legged robot. *J Intell Robot Syst* 2014; 74: 663–688.

29. Silva MF, Machado JAT and Barbosa RS. Complex-order dynamics in hexapod locomotion. *Signal Pr* 2006; 86: 2785–2793.

30. Deng H, Xin G, Zhong G, et al. Gait and trajectory rolling planning and control of hexapod robots for disaster rescue applications. *Robot Auton Syst* 2017; 95: 13–24.

31. Wang G, Chen X and Han SK. Central pattern generator and feedforward neural network-based self-adaptive gait control for a crab-like robot locomoting on complex terrain under two reflex mechanisms. *Int J Adv Robot Syst* 2017; 14: 1–13.

32. Zhang H, Zhang G and Wang J. H∞ Observer design for LPV systems with uncertain measurements on scheduling variables: application to an electric ground vehicle. *IEEE/ASME T Mech* 2016; 21: 1659–1670.

33. Wang Y, Xia Y, Member S, et al. SMC design for robust stabilization of nonlinear Markovian jump singular systems. *IEEE T Automat Contr* 2018; 63: 219.

34. Wang Y, Shen H, Karimi HR, et al. Dissipativity-based fuzzy integral sliding mode control of continuous-Time T-S fuzzy systems. *IEEE T Fuzzy Syst* 2018; 26: 1164–1176.

35. Grzelczyk D, Stańczyk B and Awrejcewicz J. Kinematics, dynamics and power consumption analysis of the hexapod robot during walking with tripod gait. *Int J Struct Stab Dy* 2017; 17: 1740010.

36. Grzelczyk D, Stańczyk B, Szymanowska O, et al. Simulation of the octopod robot controlled by different central

patterns generators. In: *Proceedings of the 14th international conference dynamical systems – theory and applications* (eds J Awrejcewicz, M Kaźmierczak, J Mrozowski, et al.), Lodz, 11–14 December 2017, pp.229–238.Singapore: Defence Science & Technology Agency.

37. Dürr V, Schmitz J and Cruse H. Behaviour-based modelling of hexapod locomotion: linking biology and technical application. *Arthropod Struct Dev* 2004; 33: 237–250.

38. Schilling M, Hoinville T, Schmitz J, et al. Walknet, a bio-inspired controller for hexapod walking. *Biol Cybern* 2013; 107: 397–419.

39. Zhao J, Zhang H, Liu Y, et al. Development of the hexapod robot HITCR-II for walking on unstructured terrain. In: *IEEE international conference on mechatronics and automation (ICMA)*, Chengdu, China, 5–8 August 2012, pp.64–69. New York: IEEE.

40. Cruse H, Kindermann T, Schumm M, et al. Walknet – a biologically inspired network to control six-legged walking. *Neural Netw* 1998; 11: 1435–1447.

41. Kuo AD. The relative roles of feedforward and feedback in the control of rhythmic movements. *Motor Control* 2002; 6: 129–145.

42. Hultborn H and Nielsen JB. Spinal control of locomotion–from cat to man. *Acta Physiol* 2007; 189: 111–121.

43. Danner SM, Hofstoetter US, Freundl B, et al. Human spinal locomotor control is based on flexibly organized burst generators. *Brain* 2015; 138: 577–588.

44. Cohen AH, Holmes PJ and Rand RH. The nature of the coupling between segmental oscillators of the lamprey spinal generator for locomotion: a mathematical model. *J Math Biol* 1982; 13: 345–369.

45. Wang T, Guo W, Li M, et al. CPG control for biped hopping robot in unpredictable environment. *J Bionic Eng* 2012; 9: 29–38.

46. de Pina Filho AC and Dutra MS. Application of hybrid van der Pol-Rayleigh oscillators for modeling of a bipedal robot. *Mech Solids Brazil* 2009; 1: 209–221.

47. Chen W, Ren G, Zhang J, et al. Smooth transition between different gaits of a hexapod robot via a central pattern generators algorithm. *J Intell Robot Syst* 2012; 67: 255–270.

48. Liu H, Jia W and Bi L. Hopf oscillator based adaptive locomotion control for a bionic quadruped robot. In: *Proceedings of the IEEE international conference on mechatronics and automation (ICMA)*, Takamatsu, Japan, 6–9 August 2017, pp.949–954. New York: IEEE.

49. Frantsevich L. Optimal leg design in a hexapod walker. *J Theor Biol* 1995; 175: 561–566.

50. Delcomyn F and Nelson ME. Architectures for a biomimetic hexapod robot. *Robot Auton Syst* 2000; 30: 5–15.

51. Jin B, Chen C and Li W. Power consumption optimization for a hexapod walking robot. *J Intell Robot Syst* 2013; 71: 195–209.

52. Nishii J. Legged insects select the optimal locomotor pattern based on the energetic cost. *Biol Cybern* 2000; 83: 435–442.

53. Nishii J. An analytical estimation of the energy cost for legged locomotion. *J Theor Biol* 2006; 238: 636–645.

54. Siregar HP. Simulation of power consumption for walking robot. In: *Proceedings of the fifth international workshop on robot motion and control, 2005 (RoMoCo '05)*, Dymaczewo, 23–25 June 2005, pp.27–32. New York: IEEE.

55. Roy SS and Pratihar DK. Effects of turning gait parameters on energy consumption and stability of a six-legged walking robot. *Rob Auton Syst* 2012; 60: 72–82.

56. De Santos PG, Garcia E, Ponticelli R, et al. Minimizing energy consumption in hexapod robots. *Adv Robot* 2009; 23: 681–704.